Hybrid-Excited Variable Reluctance Resolver with Wide Speed Range

M. Bahari, and F. Tootoonchian, *Senior Member IEEE,*

***Abstract*— The accuracy of the variable reluctance resolver (VR-Resolver) highly depends on the rotational speed and its rotational speed range is limited by the frequency of the excitation signal. To eliminate the mentioned performance dependency, this paper proposes a hybrid-excited VR-Resolver (HVR-Resolver) with two separate sets of excitation windings: a toroidal excitation winding for the AC excitation supply and an on-tooth one for the DC excitation supply. Similar to the conventional method, the HVR-Resolver is working with AC excitation ON and DC excitation OFF at the low-speed range. For high-speed operation, the excitation switched from AC excitation to DC. By using this technique, the proposed HVR-Resolver is able to accurately estimate the position at a wide speed range. This feature makes the HVR-Resolver an outstanding candidate for EV applications. The proposed design is simulated using time-stepping finite element analysis (TSFEA) in order to study the performance at both low-speed and high-speed ranges with different rotor pole numbers. In addition, an optimization process is conducted to find the best rotor shape factors. The experimental test on the proposed HVR-Resolver indicates a close agreement between simulation and experimental results.**

***Index Terms*— Hybrid-Excited Variable Reluctance Resolver (HVR-Resolver), Time-Stepping Finite Element Analysis, Toroidal Winding, Prototyped Resolver, Position Sensor.**

I. INTRODUCTION

POSITION sensors are mostly used in closed-loop control systems to deliver feedback on both the position and rotational speed of the rotary part [1]. Among different types of position sensors, optical encoders and resolvers are mostly used in different applications. The high accuracy of optical encoders made them a suitable solution for position detection. However, due to their working mechanism, they are not suitable for applications with harsh environments. On the other hand, the most known position sensor for harsh environments is resolver [2]. Resolvers have proved their robustness against environmental factors, and they are well-known for their high reliability. Between different topologies of resolvers, variable reluctance (VR) type has a smaller volume, winding less rotor, a simple manufacturing process, and acceptable accuracy [3]. Noted benefits smooth the path for VR-Resolver to widely being used in many industrial applications [4].

In recent years, electric machines are being used for various high-speed applications such as high-speed cutting, electric vehicles (EVs), grinding, and winding [5]. In addition, high-speed electric machines have other advantages such as higher power density, smaller size, and lighter weight. Employing high-speed electric machines also offers the chance for gearless electromechanical systems [6]. To this end, resolvers should be adapted with the advancement of electric machines and designed appropriately to be utilized for high-speed applications. However, there are challenges in utilizing conventional VR-Resolvers at the high-speed application, as described in Section I. A and Section I. B.

A. Dependent Speed Range

In VR-Resolvers, the injected high frequency (HF) signal is responsible to modulate the position information as the envelopes of induced voltages in signal windings. However, the frequency of the HF signal must be much higher than the frequency of mechanical rotation of the rotor, in order to maintain an acceptable accuracy. The mentioned condition limits the speed range significantly since the quality of output signals is hugely affected when the frequency of rotational speed surpasses the allowable limit [7].

B. Complex Demodulation

When the rotational speed of a conventional VR-Resolver increases, the number of samples that construct the envelopes decreases and reduces the quality of the output signals accordingly. One solution is to increase the excitation frequency to provide a reasonable number of envelope samples and maintain envelope quality [8]. Although the described solution makes the VR-Resolver a good choice for the high-speed motion control system, it requires specific integrated circuits with special processors to handle not only the huge computational burden but also the complicated demodulation procedure in order to estimate the position. Such a solution, of course, increases the complexity and cost of the RDC and the whole position detection system, simultaneously [9].

To solve the high-speed issue of the conventional VR-

M. Bahari, is with the Automation Technology and Mechanical Engineering Unit in the Faculty of Engineering and Natural Sciences at Tampere University, Tampere, Finland (Email: mohammad.bahari@alum.sharif.edu).

F. Tootoonchian is with Electrical Engineering Department, Iran University of Science and Technology (IUST), Tehran, Iran, (Email: tootoonchian@iust.ac.ir).

resolvers, Variable Reluctance Permanent Magnet Resolvers (VRPM-Resolvers) are presented in [10]-[11]. Mentioned sensors are working based on producing DC magnetic flux. In [10], signal windings have been replaced with the magnetic flux measurement unit (MFMU) to measure the flux density and convert it into output voltage through a separate magnetic flux sensor. Due to the good reliability and accuracy, measurement responsibility was left to Hall-effect sensors. Also, the excitation winding has been replaced by PMs to provide the DC flux within the sensor's body. It is worth mentioning that the information about the position of the rotor is carried by the flux itself and therefore, no demodulation technique was required. In [11], PMs have been added to the stationary part of the VR-Resolver with keeping both excitation and signal windings. At low-speed, excitation winding was supplied by a HF voltage source, but at high-speed range, the amplitude of motional back-EMF produced by PMs increased enough to induce a voltage in the signal windings. Further studies have been conducted on VRPM-Resolver in [12] to analyze the performance of the sensor in both healthy and eccentric conditions. In another study [13], a slotless axial structure was proposed for VRPM-Resolver with a leaf-style rotor for high-speed operation. To sum up, VRPM-Resolver has drawn the attention of researchers recently due to its desirable accuracy at high-speed and simple structure at the same time. Although VRPM-Resolver can operate at a wide speed range, there are several challenges in utilizing PMs in the structure of resolvers, which makes it vulnerable to harsh environmental and put doubt for using in applications such as EV, where the existence of environmental factors such as mechanical shocks, variable operating temperature, and magnetic field is undeniable:

A. PM Magnetization Characteristics Tolerance

The accuracy of the VRPM-Resolver is extremely sensitive to saturation, manufacturing tolerances, asymmetric flux distribution, and voltage imbalances. Since the magnetization characteristics of the PM play a major role in the performance of VRPM-Resolver, the main drawback of utilizing PMs is that their characteristics are subject to the manufacturing process. The tolerance in magnetization characteristics of the employed PMs creates an imbalanced flux distribution and causes position error. Apart from magnetization characteristics, identical sizes are as much important and even small differences in geometrical values of PMs could lead to position error. In [14], a difference of 1.32% in residual magnetic flux density and 2.06% in coercive force of one PM in the VRPM-Resolver caused voltage imbalance of about 10%. In addition, the average of absolute position error (AAPE) and the maximum position error (MPE) of the studied VRPM-Resolver both increased by 621% and 611%, respectively. The proposed compensation technique to prevent the potential error was to measure the magnetization characteristics of the PMs carefully before installation to minimize the possible position error [14].

B. Mechanical Robustness

Another drawback of VRPM-Resolver is related to their poor mechanical robustness. PMs in [10]-[11] are placed in the stationary part of the VRPM-Resolver. Ribs in those parts are responsible to keep the stator connected mechanically, while saturated magnetically to make the magnetic circuits of both sides isolated from each other. Rib parts are thin and fragile and as a result, locating PMs in stator teeth weakens the mechanical robustness of the sensor considerably. Since the sensor is prone to mechanical shocks and vibration in harsh industrial environments, VRPM-Resolver is not an appropriate choice for such mentioned applications.

C. Limited Operating Temperature

Changes in ambient temperature could impact the magnetization characteristics of the permanent magnets and the performance of the VRPM-Resolver as well. Permanent magnets experience a shift in flux density and coercive force as their temperature varies. When the VRPM-Resolver is heated above the maximum operating temperature of PM but below the curie temperature, it will experience an irreversible loss. After the PM of the VRPM-Resolver is heated above the curie temperature, the PM experiences permanent loss. To sum up, VRPM-Resolver operating temperature is limited by PMs temperature endurance and according to the application, it must be considered in the design procedure [15].

In addition to the above-mentioned disadvantages, the particular designs of VRPM-Resolver in each following studies have their own drawbacks as follows:

1) Since VRPM-Resolver in [10] utilized Hall-effect sensors as MFMU instead of signal windings, the magnetic flux sensors are prone to external magnetic fields, and temperature difference could cause position error as well.
2) In [11], the HF signal is injected at low-speed operation. In addition to that, the back-emf of PM at low-speed operation induces the voltage in signal windings. Extra low-speed processing is needed to filter the signal and find the rotor position by PLL. Also, the presented VRPM-Resolver cannot work in temperatures higher than 60°C, while the conventional resolver is relatively temperature resilient [16]. The mechanical strength of the studied sensor is also affected because of the ribs' existence in the stator.
3) The presented VRPM-Resolver in [17] is not capable of measuring the position of the rotary part at a standstill. Also, the position detection at lower speed is complicated and needs additional efforts such as using high-energy PM, which increases the cost of the sensor and might cause teeth saturation alongside.

In this paper, a new hybrid-excited resolver is proposed in order to overcome all the mentioned challenges. The presented structure utilizes two AC and DC excitation types, which can be turned on and turned off based on the angular velocity of the rotor. This technique guarantees high accuracy with a high pole number rotor structure at low-speed range and employs new DC-flux-based position estimation to compensate the position error of conventional position detection at high-speed range. Additionally, since there is no PM and ribs in the structure of the proposed resolver, the sensor is robust enough to be employed in applications in harsh environment such as EVs.

II. Proposed Hybrid-Excited VR Resolver

The goal of presenting the hybrid-excited variable reluctance resolver (HVR-Resolver) is to accurately estimate the position of the rotary part at a wide speed range. For this purpose, HVR-Resolver employed hybrid excitation with two different sets of excitation windings called low-speed excitation (LSE) and high-speed excitation (HSE). The LSE is supplied by a HF signal carrier and offers good performance at low-speed ranges. The LSE mode remained ON as long the mechanical rotation frequency to excitation frequency ratio is neglectable and an adequate number of samples can form the envelopes of the output signals. When the rotational speed increases and surpasses a certain threshold, the HVR-Resolver operation mode changes to HSE, in which the excitation winding is supplied with a DC source.

It should be noted the threshold for changing the operation mode is defined at a point where motional back-EMF is detectable and the accuracy of the resolver in LSE mode is not acceptable. Furthermore, since there is no PM in the structure of the proposed sensor, it solves the issues with the existing designs explained in Section I as well. The basic concept of the proposed HVR-Resolver is shown in Fig. 1.

A. Structure and Winding Configuration

The proposed HVR-Resolver has a radial flux configuration with a 12-slot stator and has three separate sets of windings. As illustrated in Fig. 2(a), its signal windings are wound toroidally around stator slots. According to the right-hand rule, the directions of signal windings are determined in the referred figure. Fig. 2(b) shows the excitation winding associated with the LSE mode and Fig. 2(c) demonstrates the excitation winding related to the HSE mode, which is supplied by a DC voltage supply to induce motional back-EMF in signal windings. The geometrical dimensions, excitation specifications, and simulation settings of the proposed HVR-Resolver are listed in Table I. As shown in Fig. 3, three different 1-X, 5-X, and 7-X rotor shapes are employed in this study.

B. Working Principle

To explain the working principle of HVR-Resolver, its operation is divided into two different parts: LSE and HSE modes. In LSE mode, the HF supply is ON and connected to the toroidal excitation winding. The voltage of the mentioned supply can be defined as V_{LSE} in (1):

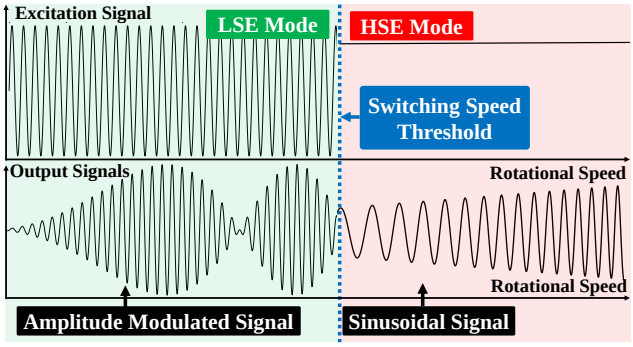

Fig. 1. The concept of the proposed HVR-Resolver.

(a) (b) (c)

Fig. 2. The winding configuration of the proposed HVR-Resolver: (a) signal coils (b) LSE toroidal coils (c) HSE on-tooth coils

(a) (b) (c)

Fig. 3. Different rotor shapes: (a) 1-X (b) 5-X (c) 7-X.

TABLE I
THE GEOMETRICAL DIMENSIONS, SIMULATION SETTINGS, MATERIAL PROPERTIES, AND EXCITATIONS OF THE HVR-RESOLVER

Parameters	Unit	Value
General Parameters		
Number of teeth	-	12
Shaft Diameter	mm	8
Stator outer/inner diameter	mm	34/24
Yoke outer/inner diameter	mm	31/27
Stator tooth width	mm	3
Stator slot depth	mm	1.5
Signal coil's turn number	-	50
HSE/LSE coil's turn number (n_{DC}/ n_{ac})	-	50
Pole Pairs, P	-	1, 5, 7
Air-gap length (min, max)	mm	0.5, 2
Simulation Settings		
Solution Type	Transient (+Adaptive Mesh)	
Stop Time	s	0.1
Time Step	us	12.5
LSE Excitation Voltage/ frequency (V_{ac}/ f_{ac})	V/Hz	5/5000
HSE Excitation Current (I_{HSE})	mA	200

$$V_{LSE} = V_{ac}\sin(\omega_{ac}t) \quad (1)$$

where V_{ac} and ω_{ac} are the amplitude and angular velocity of the LSE supply, respectively. The current passing through LSE winding can be calculated as (2):

$$I_{LSE} = \frac{V_{ac}}{\sqrt{R_{LSE}^2+\omega_{ac}^2 L_{LSE}^2}}\sin\left(\omega_{ac}t - \tan^{-1}\left(\frac{\omega_{ac}L_{LSE}}{R_{LSE}}\right)\right) \quad (2)$$

where R_{LSE} are L_{LSE} are the resistance and inductance of the LSE winding, respectively. Mutual inductances between LSE winding with signal windings can be expressed as (3)-(4):

$$L_{LSE-SIN} = L_M sin(P\theta) \quad (3)$$

$$L_{LSE-COS} = L_M cos(P\theta) \quad (4)$$

where L_M is the maximum mutual inductance and P is the number of pole pairs. Finally, the induced voltages in signal windings can be calculated as (5)-(6):

$$V_{SIN} = \frac{V_{ac}}{\sqrt{R_{LSE}^2+L_{LSE}^2}} L_M \omega_{ac} \left[P \frac{\frac{d\theta}{dt}}{\omega_{ac}} \cos(P\theta)\ \sin(\omega_{ac}t-\varphi) + \sin(P\theta)\cos(\omega_{ac}t-\varphi) \right] \quad (5)$$

$$V_{COS} = \frac{V_{ac}}{\sqrt{R_{LSE}^2+L_{LSE}^2}} L_M \omega_{ac} \left[-P \frac{\frac{d\theta}{dt}}{\omega_{ac}} \sin(P\theta)\sin(\omega_{ac}t-\varphi) + \cos(P\theta)\cos(\omega_{ac}t-\varphi) \right] \quad (6)$$

where φ is the phase difference between the voltage and current of the LSE winding. Assuming that the mechanical speed of the resolver is much lower than the excitation frequency of LSE, the induced voltages can be written as (7) and (8):

$$V_{SIN} = V_{LS} \sin(P\theta)\cos(\omega_{ac}t-\varphi) \quad (7)$$

$$V_{COS} = V_{LS} \cos(P\theta)\cos(\omega_{ac}t-\varphi) \quad (8)$$

Finally, the position of the rotary part could be decoded by demodulating the output signals and extracting the envelopes in Resolver-to-Digital Converter (RDC). The inverse tangent function is employed to estimate the position as (9):

$$\theta_{calc} = \frac{1}{P}\tan^{-1}\left(\frac{V_{LS}\sin(P\theta)}{V_{LS}\cos(P\theta)}\right) \quad (9)$$

In HSE mode, after the rotational speed of the resolver surpasses a predefined threshold, the HF supply connected to LSE turns OFF and the DC source connected to on-tooth HSE turns ON. The voltage and current of HSE are described as (10) and (11), respectively.

$$V_{HSE} = V_{DC} \quad (10)$$

$$I_{HSE} = \frac{V_{DC}}{R_{DC}} \quad (11)$$

According to the mutual inductances of signal windings in (3) and (4), the induced voltages in signal windings can be calculated for HSE mode as (12)-(13):

$$V_{SIN} = \omega_m V_{HS} \sin(P\theta) \quad (12)$$

$$V_{COS} = \omega_m V_{HS} \cos(P\theta) \quad (13)$$

where ω_m is $2\pi f_m$ and f_m is mechanical rotational frequency. It can be concluded the amplitude of induced voltages in HSE mode is proportional to the rotational speed of the resolver.

III. Performance Analysis of the HVR-Resolver

To study the performance of the HVR-Resolver in detail, time-stepping finite element analysis (TSFEA) is employed as a reliable method. The adaptive mesh refinement is applied to the proposed HVR-Resolver transient simulation in order to calculate the output signals of the studied sensor precisely. The simulation runs for one whole mechanical revolution to consider all possible sub-harmonics of the HVR-Resolver. In this section, the performance of the HVR-Resolver at both low-speed in LSE mode and high-speed in HSE mode are investigated. It is worth mentioning the 5-X shape (10 poles) rotor is considered the initial design. The time step of the simulation is chosen based on the RDC operation frequency and stop time according to one mechanical revolution.

A. At Low-Speed Range (LSE Mode)

The proposed HVR-Resolver is simulated at 600rpm with the LSE mode ON and a 5kHz carrier signal with 5V magnitude is injected into the toroidal excitation winding. The sampling frequency and stop time of the simulation are set 12.5us and 0.1s, respectively. The mutual inductance between LSE and both SIN and COS signal windings are illustrated in Fig. 4. The output signals with the extracted envelopes are shown in Fig. 5. It should be noted that the robust simple peak-detection method employed in MATLAB to calculate the envelopes. The THD of the extracted envelopes is about 0.72%. Finally, the position error of the HVR-Resolver in LSE mode is calculated and demonstrated in Fig. 6. The AAPE and MPE are 0.036° and 0.0609° respectively.

B. At High-Speed Range (HSE Mode)

To study the HVR-Resolver at high-speed, the rotational speed of the sensor is set at 18750rpm with 12.5us time step and

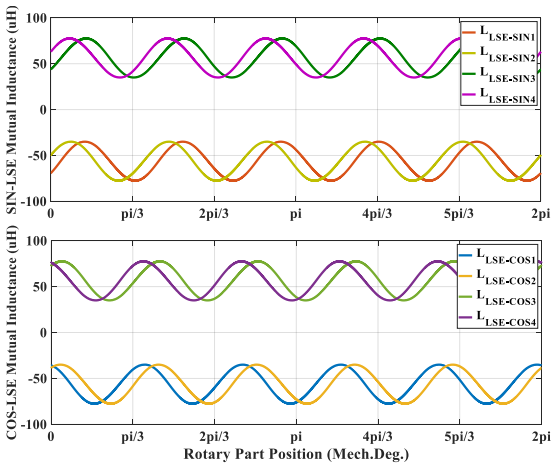

Fig. 4. Mutual inductance between LSE and signal windings.

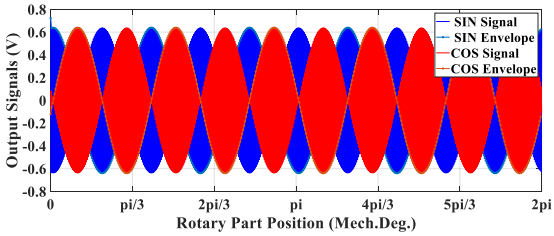

Fig. 5. Output signals in LSE mode at 600rpm.

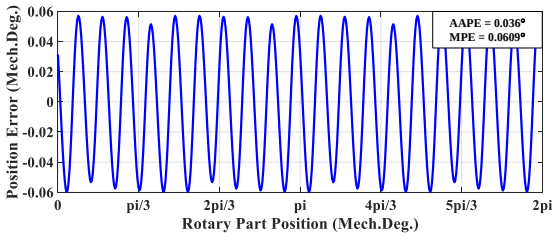

Fig. 6. Position error of HVR-Resolver in LSE mode at 600rpm.

3.2ms stop time. At this stage, the LSE mode is OFF and HSE mode is now activated to energize the on-tooth excitation coils by a 200mA DC current source. The mutual inductance between HSE and both SIN and COS signal windings are presented in Fig. 7. According to (12) and (13), the amplitude of output signals in HSE has a linear ratio with the rotational speed. The output signals are shown in Fig. 8. and their THD is about 1.63%. By comparing the real position of the rotor with the estimated position by the HVR-Resolver, the position error is computed and displayed in Fig. 9. To explain the position error, AAPE and MPE are 0.1086° and 0.1903°, respectively.

IV. Switching Speed Threshold Determination

To determine the switching threshold, first, the required conditions for switching from LSE mode to HSE mode are explained below:

1) The rotational speed increased enough to induce an adequate level of motional back-EMF in signal windings.
2) The mechanical rotational speed to excitation frequency ratio is not neglectable anymore.
3) Few samples construct envelopes of output signals in LSE mode and both the quality of signals and the accuracy of the sensor are reduced inevitably.

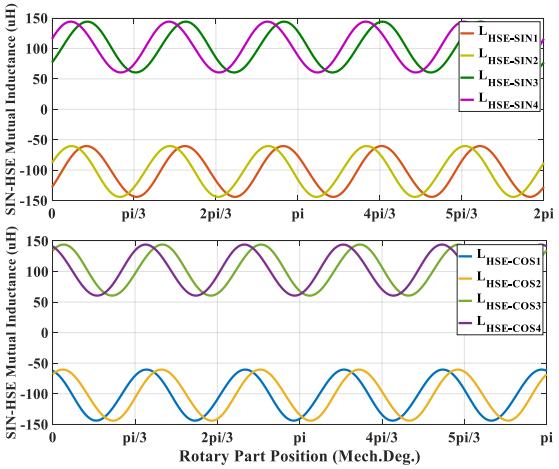

Fig. 7. Mutual inductance between LSE and signal windings.

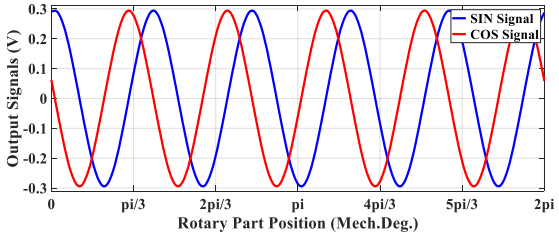

Fig. 8. Output signals in HSE mode at 18750rpm.

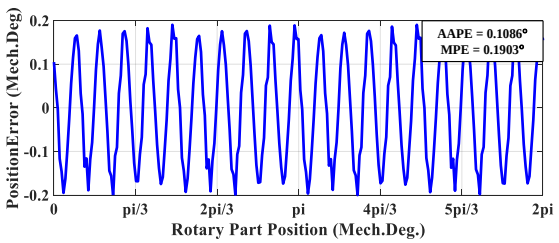

Fig. 9. Position Error of HVR-Resolver in HSE mode at 18750rpm.

Therefore, it is necessary to investigate the effect of the rotational speed on output signals in both LSE and HSE modes. Three possible rotor shapes (1-X, 5-X, and 7-X) are analyzed with the same stator. AAPE, MPE, THD of the envelopes, and level of output voltage in HSE mode are evaluated to measure the performance of the mentioned designs.

A. The Effect of Rotational Speed in LSE Mode

The proposed HVR-Resolver with different rotor designs are simulated in LSE mode at 300, 600, 1200, 1500, 2400, 3750, 7500, and 18750rpm. AAPE and MPE are considered accuracy indicators and are illustrated in Fig. 10(a) and Fig. 10(b) respectively. Furthermore, the THD of the extracted envelopes is assumed as a quality indicator of the HVR-Resolver and displayed in Fig. 10(c). The results indicate that:

1) Both accuracy and quality indicators of the 1-X HVR-Resolver have the best consistency in LSE mode. But generally, it is suffered from poor performance at a wide range of speeds (0~7500rpm) in comparison with alternative designs.
2) The performance of the 7-X HVR-Resolver highly depends on the rotational speed and its performance is getting worst at a high-speed range (from 7500rpm and above). But both the accuracy and the quality parameters of the mentioned resolver are ideal at low-speed ranges (0~7500rpm).
3) By employing LSE and HSE modes, the sensor can take the benefits of the ideal accuracy and quality of the 7-X rotor design at low-speed. So, before the performance of

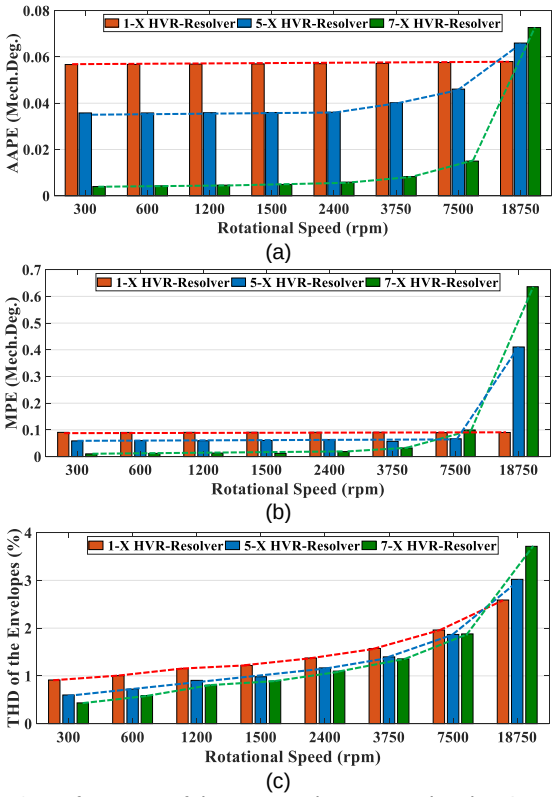

Fig. 10. Performance of the proposed HVR-Resolver in LSE mode with various rotor shapes at different rotational speeds: (a) AAPE (b) MPE (c)THD

the 7-X HVR-Resolver is affected by high rotational speed, the excitation mode must switch to HSE mode.

B. The Effect of Rotational Speed in HSE Mode

In this section, the efficacy of the HVR-Resolver in HSE mode at different rotational speeds is evaluated. AAPE and MPE as accuracy indicators are illustrated for different rotor designs in Fig. 11(a) and Fig. 11(b), respectively. THD of the envelopes, as a quality indicator, is shown in Fig. 11(c). In addition to the mentioned indicators, the maximum output voltage is added to the study and shown in Fig. 11(d) to make sure that the level of motional back-EMF signals is high enough and readable for the RDC. The following conclusion could be drawn from analyzing the studied resolver in HSE mode:

1) For 5-X and 7-X HVR-Resolver, the level of motional back-EMF is acceptable for position detection system from 2400rpm, while for 1-X HVR-Resolver, rotational speed should at least increase to 9600rpm.
2) Among three different rotor shapes, 7-X HVR-Resolver has the best performance and highest accuracy and quality indicator values.

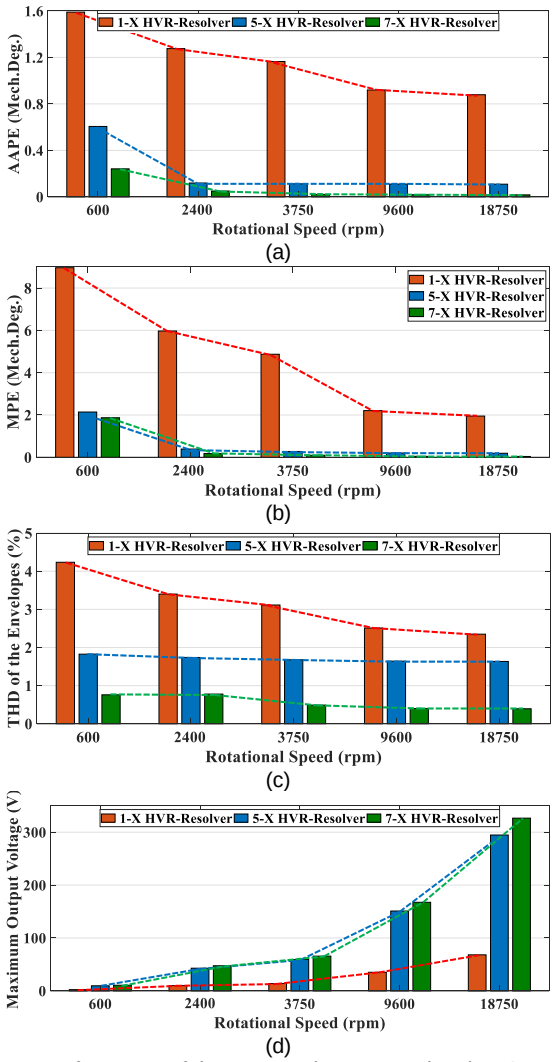

Fig. 11. Performance of the proposed HVR-Resolver in HSE mode with various rotor shapes at different rotational speeds: (a) AAPE (b) MPE (c)THD (d) maximum voltage signal.

3) The 7-X HVR-Resolver is the best candidate since it shows ideal accuracy in LSE mode at low-speed ranges and consistent performance in HSE mode at high-speed ranges.

C. Determining the Switching Speed Threshold

After investigating the performance of the HVR-Resolver in both LSE and HSE mode at a wide speed range with different rotor pole pairs, 12-slot 7-X HVR-Resolver is chosen as the best design because of its excellent accuracy and quality indicator values and chosen for further study. To determine the switching threshold, the speed range of LSE for this particular design should be limited. For this purpose, a standard number of samples in each electrical period is defined to pave the way for high-quality envelopes. At least 16 samples in each electrical period of output signals are essential to keep both the accuracy and the quality parameters of the resolver in LSE mode at a decent level. Consequently, the switching threshold is set at 2400rpm for 7-X HVR-Resolver to keep the performance of the sensor acceptable at a wide speed range.

V. Geometrical Optimization on Rotor Shape Factors

Rotor shape factors play a major role in the performance of the HVR-Resolver. The 12-slot 7-X HVR-Resolver is analyzed using TSFEA with different rotor shape factors to achieve the optimal design. All simulations are done in LSE mode at 600rpm and both accuracy and quality indicators are examined to evaluate the performance. Two G_{min} and G_{max} parameters are defined as minimum and maximum air-gap lengths. The shape of the rotor is designed so that the permeance of the air-gap varies sinusoidally with different G_{min} and G_{max} combinations. The lowest value for the G_{min} range is considered 0.5mm due to the mechanical limitation of airgap and the highest value for the G_{max} range is considered 3mm. All the necessary criteria and constraints are considered to find the appropriate design. The constraints of the optimization problem are defined below:

- Designs with $G_{max} \leq G_{min}$
- Designs with $G_{max} > 3^{mm}$
- Designs with AAPE>0.1°, MPE>0.1°, $V<0.1^{V}$, or THD>2%

Mentioned designs are considered unacceptable or highlighted in red due to their unsatisfactory performance. The objective function of the optimization takes both accuracy and quality indicators into account and considers the level of output voltages as a constraint.

A. Accuracy Indicators

Different combinations are examined with 0.25mm intervals. Fig. 12(a) and Fig. 12(b) are illustrating the AAPE and MPE of the studied HVR-Resolver, respectively, as accuracy indicators. Ideal designs are highlighted green and designs with poor performance are highlighted red.

B. Quality Indicator

After extracting the envelopes from output voltages, the THD of signals is calculated and shown in Fig. 13(a). Also, the maximum amplitude of output voltage envelopes, which is a decisive parameter, is illustrated in Fig. 13(b).

The scalar cost function (CF) is formed with a weighting vector (K) in (14) and (15):

$$CF = K^T C \tag{14}$$

$$K = [k_1 \;\; k_2 \;\; k_3 \;\; k_4]^T \in \mathbb{R}^3 \tag{15}$$

and a vector of four criteria are in (16):

$$C = [c_1 \;\; c_2 \;\; c_3 \;\; c_3]^T \in \mathbb{R}^3 \tag{16}$$

where the criteria are described in Section V. A and Section V. B. The cost function values are calculated and displayed in Fig. 14 for different designs.

VI. Experimental Results

To verify the performance of the proposed HVR-Resolver in two LSE and HSE modes, the prototype of the 12-slot stator with the optimal rotor shape is built. The stator core, optimal 7-X shape rotor, and wound stator are shown in Fig. 15(a) through Fig. 15(c), respectively. In addition to signal windings, two separate LSE and HSE windings are wounded in toroidal and on-tooth, respectively. To rotate the resolver at different rotational speeds, a controllable DC motor is employed, and a precise optical encoder is installed on the shaft of the motor as a position reference. The experimental setup is shown in Fig. 16 and a digital oscilloscope is employed to capture the output signals of the studied HVR-Resolver. The measured signals are imported into MATLAB software to process them and find the estimated position and compare it to the reference position. The position estimation in the experimental test is divided into two different LSE and HSE modes:

A. LSE mode

In LSE mode, the toroidally-wound LSE winding is fed by a synthesized function generator. It should be noted the resolution

AAPE (Mech.Deg.) of HVR-Resolver for Different Rotor G_{min} and G_{max}

G_{min} of 7-X Rotor Shape (mm) \ G_{max} of 7-X Rotor Shape (mm)	0.75	1.00	1.25	1.50	1.75	2.00	2.25	2.50	2.75	3.00
0.50	0.0096	0.0124	0.0058	0.0033	0.0024	0.004	0.0059	0.0073	0.0079	0.0083
0.75		0.0169	0.0145	0.0069	0.0048	0.0064	0.0074	0.0073	0.0073	0.0074
1.00			0.0123	0.0166	0.009	0.0065	0.0063	0.0067	0.0067	0.0066
1.25				0.0142	0.0399	0.0108	0.0064	0.0065	0.0057	0.0054
1.50					0.0181	0.0413	0.0107	0.0176	0.0104	0.0097
1.75						0.0233	0.0945	0.015	0.0105	0.0099
2.00							0.0313	0.1098	0.035	0.0134
2.25								0.0418	0.1336	0.0528
2.50									0.0546	0.1629
2.75										0.0737

AAPE<0.005 ° Ideal
AAPE<0.01°
AAPE<0.02°
AAPE>0.1° Poor
Unacceptable Range

(a)

MPE (Mech.Deg.) of HVR-Resolver for Different Rotor G_{min} and G_{max}

G_{min} of 7-X Rotor Shape (mm) \ G_{max} of 7-X Rotor Shape (mm)	0.75	1.00	1.25	1.50	1.75	2.00	2.25	2.50	2.75	3.00
0.50	0.0318	0.0339	0.018	0.0169	0.0142	0.0141	0.015	0.0166	0.0162	0.0177
0.75		0.0522	0.037	0.0234	0.0379	0.0364	0.0366	0.0352	0.0347	0.0337
1.00			0.066	0.0439	0.037	0.0323	0.0371	0.0369	0.0394	0.0379
1.25				0.0807	0.1067	0.0592	0.04	0.0315	0.0323	0.0322
1.50					0.1133	0.1167	0.0708	0.0781	0.0513	0.0502
1.75						0.1703	0.2053	0.0788	0.0733	0.0671
2.00							0.2431	0.2494	0.1453	0.0909
2.25								0.3373	0.3351	0.1907
2.50									0.4277	0.4381
2.75										0.6021

MPE<0.02 ° Ideal
MPE<0.03°
MPE<0.04°
MPE>0.1° Poor
Unacceptable Range

(b)

Fig. 12. Accuracy indicators of the HVR-Resolver with different rotor shape factors: (a) AAPE (b) MPE.

Envelopes THD (%) of HVR-Resolver for Different Rotor G_{min} and G_{max}

G_{min} of 7-X Rotor Shape (mm) \ G_{max} of 7-X Rotor Shape (mm)	0.75	1.00	1.25	1.50	1.75	2.00	2.25	2.50	2.75	3.00
0.50	1.8496	1.8794	1.8556	1.8573	1.8647	1.8696	1.8692	1.8698	1.8726	1.877
0.75		1.8659	1.8895	1.8643	1.8563	1.8498	1.8489	1.8496	1.8507	1.8524
1.00			1.8889	1.9004	1.8788	1.8727	1.8611	1.8582	1.857	1.8586
1.25				1.9119	1.8568	1.886	1.8809	1.8895	1.8699	1.8738
1.50					1.9352	1.8654	1.9028	1.8793	1.8841	1.8895
1.75						1.9701	1.9959	1.9305	1.9109	1.9058
2.00							2.0467	2.0492	1.9582	1.8944
2.25								2.1484	2.151	2.0139
2.50									2.3329	2.2886
2.75										2.6018

THD > 2% Poor
Unacceptable Range

(a)

Maximum Voltage (V) of HVR-Resolver for Different Rotor G_{min} and G_{max}

G_{min} of 7-X Rotor Shape (mm) \ G_{max} of 7-X Rotor Shape (mm)	0.75	1.00	1.25	1.50	1.75	2.00	2.25	2.50	2.75	3.00
0.50	0.2187	0.3476	0.4295	0.4839	0.5211	0.5471	0.5656	0.5791	0.5893	0.5974
0.75		0.1334	0.2197	0.278	0.3186	0.347	0.3673	0.3822	0.3929	0.4009
1.00			0.0887	0.1483	0.1901	0.2204	0.2419	0.2572	0.2683	0.2766
1.25				0.0615	0.1038	0.1342	0.1568	0.1728	0.1843	0.1927
1.50					0.0437	0.0743	0.097	0.1134	0.1255	0.1341
1.75						0.0316	0.0538	0.0709	0.0831	0.0921
2.00							0.0231	0.0394	0.0524	0.0614
2.25								0.017	0.0291	0.0388
2.50									0.0125	0.0214
2.75										0.0093

V > 0.5V Ideal
V > 0.4V
V > 0.3V
V < 0.1V Poor
Unacceptable Range

(b)

Fig. 13. Quality indicators of the HVR-Resolver with different rotor shape factors: (a) THD (b) maximum voltage.

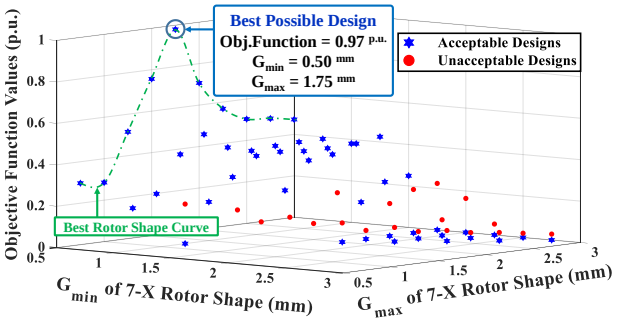

Fig. 14. Objective function values of the optimization.

(a) (b) (c)

Fig. 15. The prototype resolver: (a) the stator core, (b) the rotor, and (c) the wound stator

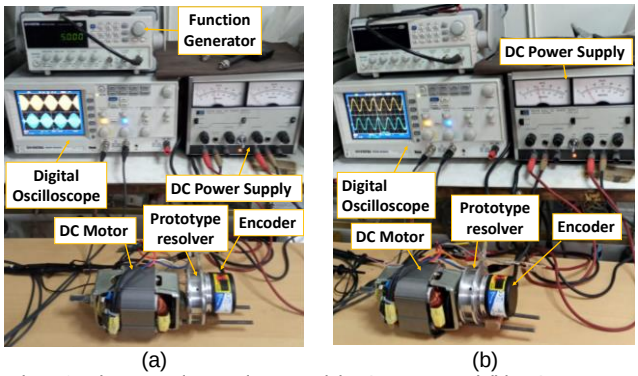

(a) (b)

Fig. 16. The experimental setup: (a) LSE test, and (b) HSE test

of the employed function generator is 0.1Hz and the automatic gain control circuit adjust its voltage amplitude. The peak detection method is responsible for extracting the envelopes of the captured signals and the inverse tangent function is applied on the SIN to COS envelopes ratio to estimate position. In LSE mode, the prototyped HVR-Resolver is tested at 600 rpm, 1200 rpm, and 2400 rpm. The results are listed in Table II and compared with the TSFEA results.

B. HSE mode

When the rotational speed surpasses the defined switching speed threshold, the LSE turns OFF and the DC supply turns on to supply the HSE winding. Also, the inverse tangent function is applied to the SIN to COS signals ratio, after they are imported into MATLAB. The prototyped sensor is tested at 2400 rpm, 3750 rpm, and 9600 rpm in HSE mode. The results in comparison with those of TSFEA are listed in Table II.

As given in Table II, the experimental results are in close agreement with the predicted values that approve the success of the proposed design.

VII. Conclusion

The main purpose and contribution of this paper is to propose a hybrid-excited concept for VR-Resolvers. As described in Section II. A, two different sets of winding excitation connected to AC and DC sources were used. Two modes called LSE and HSE were employed for low- and high-speed ranges, in which the excitation type would switch according to the Switching Speed Threshold (Section II. B). The presented HVR-Resolver has advantages compared to the existing designs as follows:

1. Since the output signals of the sensor at HSE mode are the envelopes, no demodulation process is required, and the computational cost of position calculation is reduced (Section III. B).
2. The high number of pole pairs, which guarantees ideal position detection accuracy at a low-speed range, can be employed (Section IV. A).
3. With the advantage of motional back-EMF in HSE mode, both accuracy and quality indicators are improved significantly at high-speed ranges (Section IV. B).
4. HVR-Resolver has no PM and ribs in its structure and as a result, in comparison with PM-Resolvers, its robustness against high temperature, mechanical shocks, vibration, and an external magnetic field is improved considerably.
5. With the combination of LSE and HSE modes, the presented HVR-Resolver can measure the position at a wide speed range.

References

[1] H. Saneie and Z. Nasiri-Gheidari, "Generalized Nonoverlapping Tooth Coil Winding Method for Variable Reluctance Resolvers," in *IEEE Transactions on Industrial Electronics*, vol. 69, no. 5, pp. 5325-5332, May 2022, doi: 10.1109/TIE.2021.3084157.

[2] X. Ge, Z. Q. Zhu, R. Ren and J. T. Chen, "A Novel Variable Reluctance Resolver for HEV/EV Applications," in *IEEE Transactions on Industry Applications*, vol. 52, no. 4, pp. 2872-2880, July-Aug. 2016.10.1109/TIA.2016.2533600.

[3] F. Zare, A. Keyvannia and Z. Nasiri-Gheidari, "Presentation of a Novel Variable-Reluctance Tubular Resolver," in *IEEE Transactions on Industrial Electronics*, doi: 10.1109/TIE.2022.3146595.

[4] X. Ge, Z. Q. Zhu, R. Ren and J. T. Chen, "Analysis of Windings in Variable Reluctance Resolver," in *IEEE Transactions on Magnetics*, vol. 51, no. 5, pp. 1-10, May 2015, Art no. 8104810.

[5] N. Bianchi, S. Bolognani and F. Luise, "Potentials and limits of high-speed PM motors," in *IEEE Transactions on Industry Applications*, vol. 40, no. 6, pp. 1570-1578, Nov.-Dec. 2004.

[6] Li, Silong. (2016). High-Speed Electric Machines: Challenges and Design Considerations. *IEEE Transactions on Transportation Electrification*. 2. 2-13. 10.1109/TTE.2016.2523879.

[7] Bahari, M., Nasiri-Gheidari, Z. The Comparative Analysis of AC-Flux and DC- Flux Resolvers. *Scientia Iranica*, 2020.

[8] M. Caruso, A. O. Di Tommaso, F. Genduso, R. Miceli and G. R. Galluzzo, "A DSP-Based Resolver-To-Digital Converter for High-Performance Electrical Drive Applications," in *IEEE Transactions on Industrial Electronics*, vol. 63, no. 7, pp. 4042-4051, July 2016.

[9] M. Kozovsky, P. Blaha, "High Speed Operation Tests of Resolver Using AURIX Microcontroller Interface", *IFAC-PapersOnLine*, Volume 51, Issue 6, 2018, Pages 384-389, ISSN 2405-8963.

[10] M. Bahari, A. Davoodi, H. Saneie, F. Tootoonchian and Z. Nasiri-Gheidari, "A New Variable Reluctance PM-Resolver," in *IEEE Sensors Journal*, vol. 20, no. 1, pp. 135-142, 1 Jan.1, 2020.

[11] L. Sun, J. Taylor, A. D. Callegaro and A. Emadi, "Stator-PM-Based Variable Reluctance Resolver with Advantage of Motional Back-EMF," in *IEEE Transactions on Industrial Electronics*, vol. 67, no. 11, pp. 9790-9801, Nov. 2020.

[12] P. Naderi, R. Ghandehari and M. Heidary, "A Comprehensive Analysis on the Healthy and Faulty Two Types VR-Resolvers with Eccentricity and Inter-Turn Faults," in *IEEE Transactions on Energy Conversion*, vol. 36, no. 4, pp. 3502-3511, Dec. 2021.

[13] L. Sun, Z. Luo, J. Hang, S. Ding and W. Wang, "A Slotless PM Variable Reluctance Resolver with Axial Magnetic Field," in *IEEE Transactions on Industrial Electronics*, vol. 69, no. 6, pp. 6329-6340, June 2022.

[14] M. Bahari, F. Tootoonchian and A. Mahmoudi, "An Electromagnetic Design of Slotless Variable Reluctance PM-Resolver," in *IEEE Transactions on Industrial Electronics*, vol. 70, no. 5, pp. 5336-5346, May 2023.

[15] V. Ghorbanian, S. Hussain, S. Hamidizadeh, R. Chromik and D. Lowther, "The Role of Temperature-Dependent Material Properties in Optimizing the Design of Permanent Magnet Motors," in *IEEE Transactions on Magnetics*, vol. 54, no. 3, pp. 1-4, March 2018, Art no. 8101104.

[16] Petchmaneelumka, W.; Riewruja, V.; Songsuwankit, K.; Rerkratn, A. A Temperature Compensation Technique for Improving Resolver Accuracy, *Sensors 2021*, 21, 6069.

[17] R. Ghandehari, P. Naderi and L. Vandevelde, "Performance Analysis of a New Type PM-Resolver in Healthy and Eccentric Cases by an Improved Parametric MEC Method," in *IEEE Transactions on Instrumentation and Measurement*, vol. 70, pp. 1-10, 2021, Art no. 1503610.

Table II. Comparing the experimental results with those of TSFEA in low-speed and high-speed operation

Mode	Rotational Speed (rpm)	AAPE (Arc min.)			MPE (Arc min.)			THD of Envelopes (%)		
		TSFEA	Measured	Deviation (%)	TSFEA	Measured	Deviation (%)	TSFEA	Measured	Deviation (%)
LSE-ON HSE-OFF	600	0.24	0.25	4	0.72	0.78	7.69	0.59	0.62	4.84
	1200	0.30	0.32	6.25	0.78	0.82	4.88	0.81	0.85	4.71
	2400	0.36	0.38	5.26	1.14	1.18	3.39	1.10	1.18	6.78
HSE-ON LSE-OFF	2400	2.46	2.52	2.38	11.40	11.92	4.36	0.73	0.77	5.19
	3750	1.26	1.32	4.55	5.70	5.98	4.68	0.49	0.52	5.77
	9600	1.08	1.15	6.09	2.64	2.81	6.05	0.40	0.43	6.98